The Canadian Mineralogist
Vol. 33, pp. 1011-1022 (1995)

OLIVINE OIKOCRYSTS IN BUSHVELD ANORTHOSITE: SOME IMPLICATIONS FOR CUMULATE FORMATION

WOLFGANG D. MAIER

Sciences de la Terre, Université du Québec, Chicoutimi, Québec G7H 2B1

ABSTRACT

Samples of anorthosite from the Bushveld Complex, in South Africa, characteristically contain oikocrysts that are colloquially known as "mottles". In most cases, oikocrysts are ortho- or clinopyroxene. In this study, I describe an occurrence of mottles containing abundant olivine, amphibole, and mica in addition to orthopyroxene and plagioclase. The olivine oikocrysts enclose numerous small, rounded, and embayed grains of plagioclase. These inclusions are compositionally markedly different from plagioclase in the host anorthosite, which rules out a heteradcumulate origin for the mottles. Both inclusions and plagioclase of the host anorthosite are compositionally reversely zoned. A Ca-rich rim (up to An_{95}) is attributed to partial resorption by an interstitial melt enriched in H_2O.

Keywords: anorthosite, cumulate, texture, resorption, oikocrysts, Bushveld Complex, South Africa.

SOMMAIRE

Des échantillons d'anorthosite provenant du complexe de Bushveld, en Afrique du Sud, contiennent de façon caractéristique des oïkocristaux en taches que l'on appelle couramment "mottles". Dans la plupart des cas, ces oïkocristaux sont soit de l'orthopyroxène, soit du clinopyroxène. Ce travail porte sur un exemple de tache contenant une abondance d'olivine, d'amphibole et de mica, aussi bien que d'orthopyroxène et de plagioclase. Les oïkocristaux à olivine englobent de nombreux petits cristaux de plagioclase arrondis et résorbés. Ceux-ci ont une composition très différente de celle du plagioclase dans l'anorthosite encaissante, ce qui élimine une origine hétéradcumulative. Ces inclusions, aussi bien que le plagioclase de la roche hôte, montrent une zonation inversée. Le développement d'une bordure calcique (jusqu'à An_{95}) résulterait d'une résorption partielle dans un liquide interstitiel enrichi en H_2O.

(Traduit par la Rédaction)

Mots-clés: anorthosite, cumulats, texture, résorption, oïkocristaux, complexe de Bushveld, Afrique du Sud.

INTRODUCTION

Within the last decade, classical interpretations of cumulates have been increasingly questioned. Wager *et al.* (1960) classified cumulus rocks into ad-, meso-, and orthocumulates, on the basis of an increasing relative proportion of intercumulus material. However, in many cases, the genetic conotations of the terms "cumulus" and "intercumulus" have been found to be impractical. Hence, whereas Raedeke & McCallum (1980) proposed that oikocrysts in the Stillwater Complex are a product of trapped intercumulus melt, studies on pyroxene oikocrysts of the Skaergaard intrusion (McBirney & Noyes 1979, McBirney & Hunter 1995) and of some Australian layered intrusions (Mathison 1987) suggest that cumulus and intercumulus material may crystallize simultanously at a crystallization front.

Intercumulus oikocrysts are also a characteristic feature of anorthosite in the Bushveld Complex (Wager & Brown 1968, p. 359; Maier 1992). As in other layered complexes, most oikocrysts consist of orthopyroxene and clinopyroxene. This investigation focusses on oikocrysts of olivine and compares them to the more common pyroxene oikocrysts. Olivine oikocrysts have not been described in the literature so far, but they may have important implications for cumulate formation.

The anorthosite that hosts the olivine oikocryst discussed here occurs toward the top of the Upper Critical Zone of the Western Bushveld Complex, at Impala Platinum Mines, Wildebeestfontein North Section (Fig. 1). The layer is 10 m thick and overlies the UG2 chromitite and pyroxenite. Similar oikocrysts were observed within the UG2 – Merensky Reef interval at two other localities in the Western Bushveld Complex.

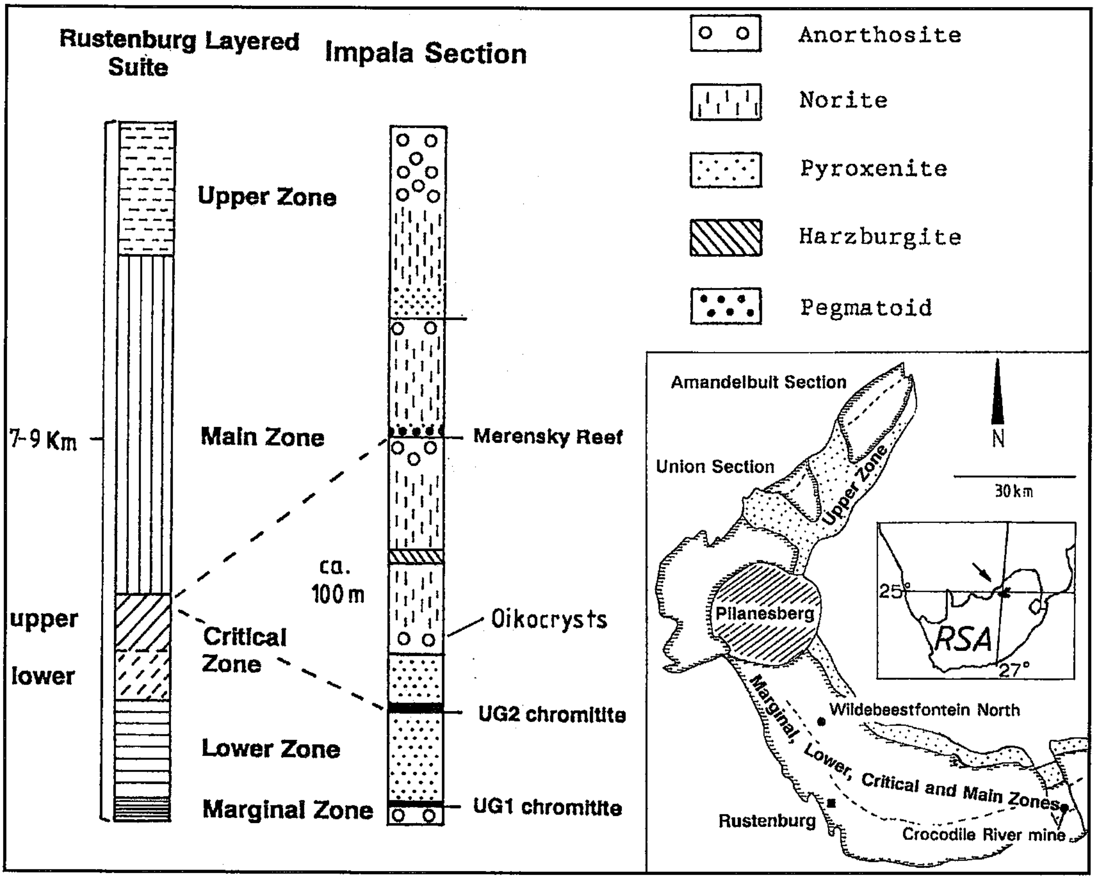

FIG. 1. Stratigraphic subdivision of the Rustenburg Layered Suite, and generalized section through the Upper Critical Zone at Impala Platinum Mines, Wildebeestfontein North Section. Map shows the western lobe of the Bushveld Complex. The dashed line indicates the sub-outcrop position of the Merensky Reef.

PETROGRAPHY

Samples of anorthosite in the Upper Critical Zone of the Bushveld Complex generally contain between 0 and 10% interstitial material. As such, most of them may be classified as plagioclase adcumulate (Wager *et al.* 1960). Most of the interstitial material is ortho- and clinopyroxene, which occur in the form of oikocrysts containing numerous chadacrysts of plagioclase. Oikocrysts are generally distributed evenly in the rock, with the distance between individual oikocrysts being usually *ca.* 5 to 10 cm. Where ortho- and clinopyroxene occur together, the former is generally surrounded by a zone of poikilitic clinopyroxene. Such aggregates of interstitial orthopyroxene and clinopyroxene are commonly referred to as "mottles" in the literature on the Bushveld Complex. Mottles that are made up of oikocrystic olivine are less common; I have observed them, other than in the example selected for detailed study, in the Amandelbult Section (borehole intersection 7E^3, Maier 1992), where they occur at the same stratigraphic position as at the Impala mine, and below the UG2 chromitite at the Crocodile River mine (Fig. 1).

The olivine mottle studied in detail is shown in Figure 2. The core of the mottle consists of a complex intergrowth of olivine, orthopyroxene, and plagioclase. Olivine is in optical continuity. Laths of partially chloritized phlogopite (Fig. 3a), with their long dimensions oriented subparallel to the layering, cut across grain boundaries; they are associated mainly with orthopyroxene and may be attributed to replacement as a result of reaction of the pyroxene with a late-stage liquid. The oikocrystic olivine and orthopyroxene are anhedral and poikilitically enclose numerous rounded,

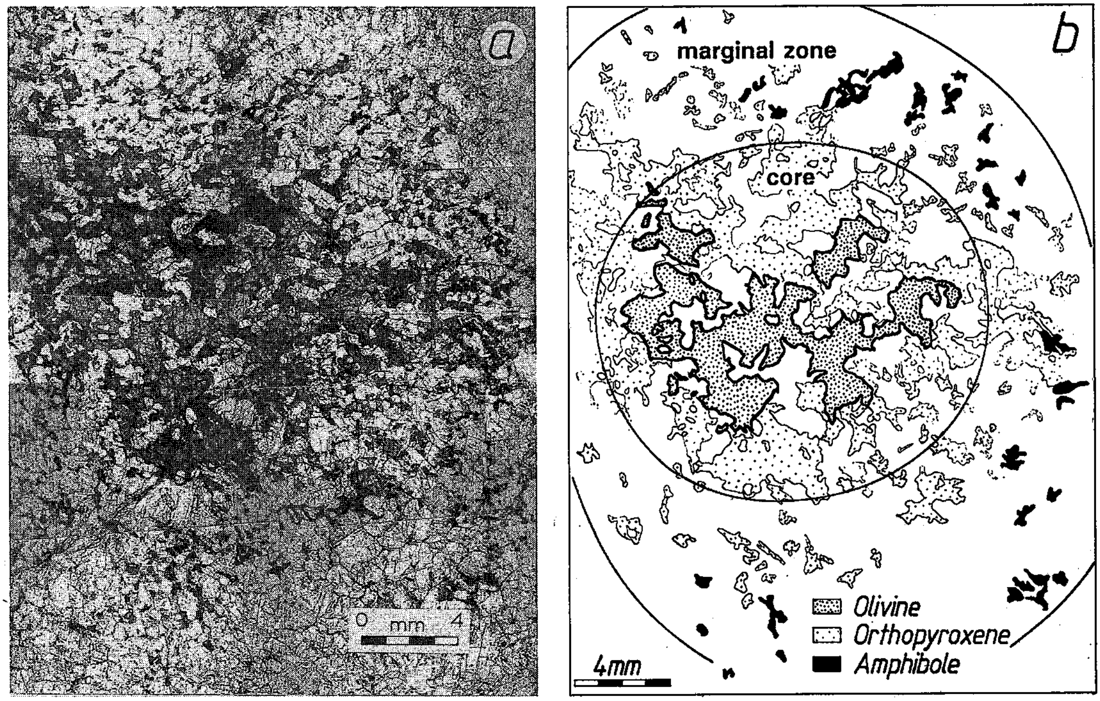

FIG. 2. (a) Photomicrograph and (b) sketch map of the olivine mottle analyzed. Note that the boundary between core and marginal zone is gradational rather than precisely defined.

anhedral grains of plagioclase (Figs. 3b, c, d, e). Many of the grains are irregularly embayed (Fig. 3e). A narrow zone consisting of amphibole (Figs. 3d, e) or, less commonly, an unidentified, fibrous phase, is generally developed between plagioclase and olivine. About 10% of the olivine and orthopyroxene in the core area is serpentinized.

The core of the mottle is surrounded by a marginal zone (Fig. 2b) of relatively fine-grained subhedral plagioclase (*ca.* 80 vol.%), interstitial orthopyroxene and hornblende (both *ca.* 10 vol.%), and minor phlogopite and quartz. With increasing distance from the core, the marginal zone grades into a laminated anorthosite largely free of interstitial pyroxene and amphibole: plagioclase domains become progressively larger and more tabular, and the rock displays triple-point junctions. Grain sizes within the anorthosite are similar to those of other samples of anorthosite and norite in the UG2 – Merensky Reef interval (Maier 1994).

Modal analysis of the mottle gave the following volume proportions (note that values are approximate, as the borders of the mottle cannot be defined precisely): plagioclase 67%, orthopyroxene 17%, olivine 8%, amphibole 3%, serpentine 3%, mica 1.5%, quartz 0.5%.

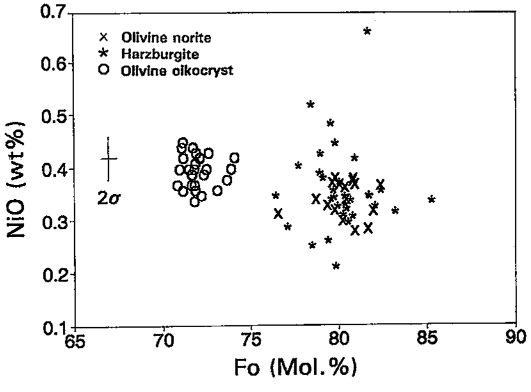

FIG. 4. Levels of NiO plotted against Fo content in olivine, based on electron-microprobe analysis of 49 samples from the UG2 chromitite – Merensky Reef interval in the Western Bushveld Complex (Maier 1992). Error bars depict 2σ standard deviation of analytical precision derived from 10 closely spaced analyses of an olivine secondary standard.

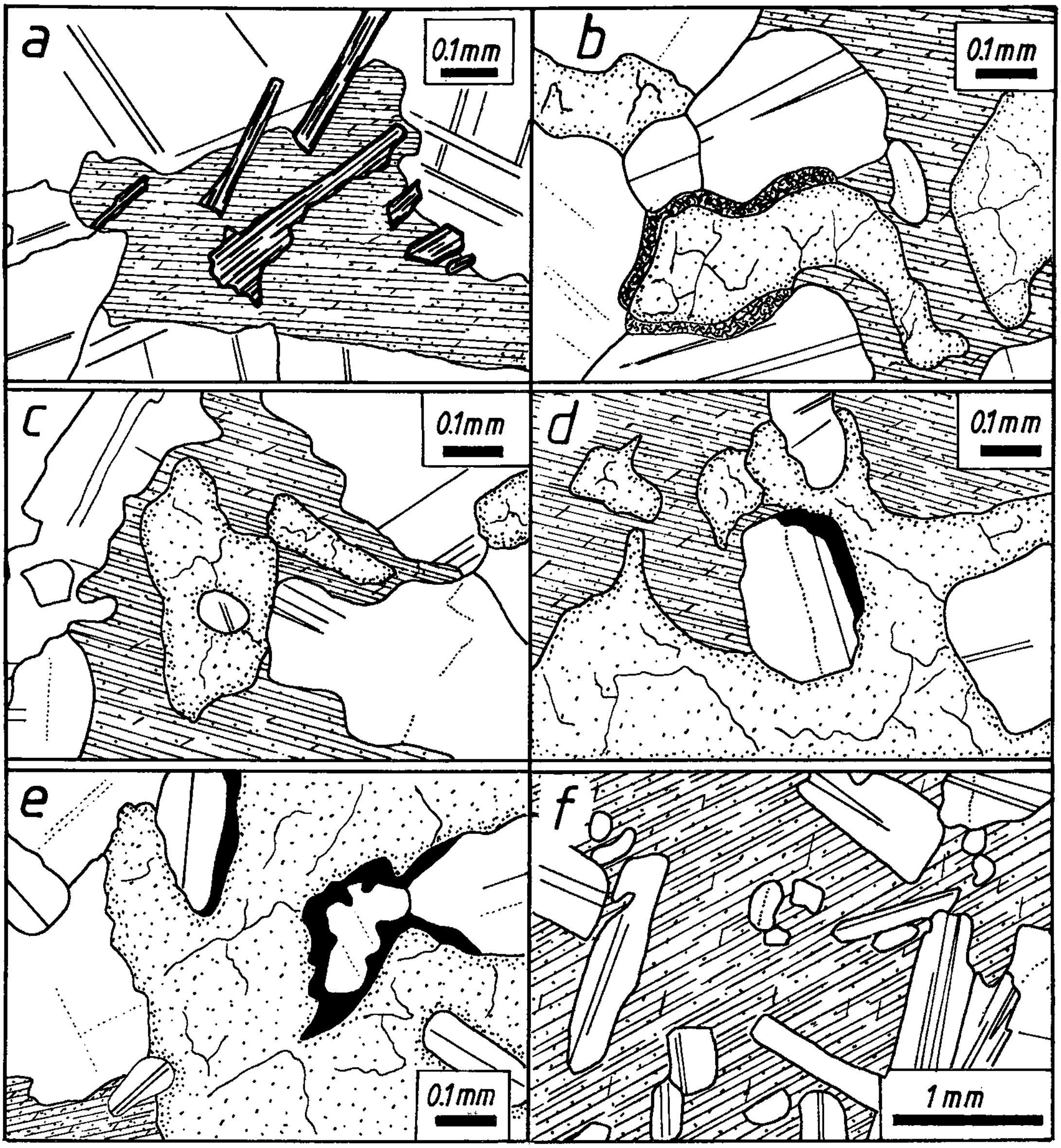

FIG. 3. (a) Phlogopite laths (bold) originating in orthopyroxene (striped). Matrix is plagioclase (twinning is idealized for clarity). (b, c) Subrounded and rounded inclusions of plagioclase in anhedral olivine (stippled) and orthopyroxene. Note the corona of an unidentified fibrous phase (patterned) around olivine in (b). (d, e) Plagioclase inclusions in olivine rimmed by amphibole (solid). (f) Inclusions of plagioclase in orthopyroxene oikocryst. Note the change in scale. To enhance clarity, these figures have been traced from photomicrographs.

MINERAL CHEMISTRY

All analyses were performed on a JEOL CXA–733 electron microprobe at Rhodes University, using a defocused 10 μm beam, an acceleration potential of 15 kV, and a beam current of 25 nA.

The olivine in the core of the mottle contains between 36 and 38 wt% MgO (Fo_{71} – Fo_{74}), with no significant zonation being detectable. The Ni content of the olivine is approximately 0.4 wt% NiO. In comparison, olivine from harzburgite and olivine norite in the UG2 – Merensky Reef interval is

TABLE 1. COMPOSITION OF ORTHOPYROXENE IN THE OLIVINE MOTTLE

Analysis	1	2	3	4	5	6	7	8	9	10	11	12	13	14	15	16	17
Type	o	o	+	+	+	+	+	+	+	+	+	o	+	+	o	o	o
SiO2	53.24	53.44	53.34	53.37	53.74	53.80	53.69	53.65	53.82	53.94	53.93	53.09	54.01	53.87	53.36	53.42	53.44
TiO2	0.18	0.19	0.20	0.13	0.11	0.11	0.17	0.12	0.12	0.09	0.17	0.21	0.10	0.20	0.21	0.22	0.26
Al2O3	0.94	1.19	1.89	1.74	1.74	1.73	1.54	1.97	1.80	1.82	1.66	1.06	1.84	1.44	1.23	0.96	0.83
Cr2O3	0.22	0.25	0.23	0.19	0.07	0.11	0.17	0.18	0.05	0.13	0.26	0.20	0.13	0.13	0.21	0.20	0.16
FeO	18.72	17.38	16.02	15.55	15.60	15.56	15.38	15.48	15.51	15.51	16.23	19.05	16.02	15.95	18.05	18.46	19.34
MnO	0.34	0.22	0.22	0.25	0.19	0.18	0.22	0.21	0.21	0.20	0.23	0.30	0.22	0.29	0.30	0.29	0.33
NiO	0.11	0.14	0.12	0.11	0.09	0.08	0.09	0.05	0.11	0.12	0.06	0.10	0.09	0.07	0.06	0.13	0.13
MgO	24.62	25.88	26.96	27.22	27.89	27.72	27.36	27.86	27.75	27.83	26.97	24.94	27.43	27.14	25.30	25.41	24.45
CaO	0.77	0.67	0.47	0.42	0.45	0.49	0.78	0.32	0.47	0.35	0.49	0.93	0.31	0.70	0.81	0.71	0.81
Na2O	0.01	0.00	0.00	0.00	0.00	0.00	0.00	0.00	0.00	0.00	0.01	0.02	0.00	0.00	0.01	0.01	0.00
Total	99.14	99.36	99.45	98.97	99.86	99.76	99.41	99.86	99.83	100.00	100.03	99.89	100.15	99.78	99.55	99.79	99.74
Cations (based on 6 atoms of oxygen) :																	
Si	1.97	1.96	1.94	1.95	1.94	1.94	1.95	1.94	1.94	1.94	1.95	1.95	1.95	1.95	1.96	1.96	1.97
Ti	0.01	0.01	0.01	0.00	0.00	0.00	0.00	0.00	0.00	0.00	0.00	0.01	0.00	0.01	0.01	0.01	0.01
Al	0.04	0.05	0.08	0.07	0.07	0.07	0.07	0.08	0.08	0.08	0.07	0.05	0.08	0.06	0.05	0.04	0.04
Cr	0.01	0.01	0.01	0.01	0.00	0.00	0.00	0.01	0.00	0.00	0.01	0.01	0.00	0.00	0.01	0.01	0.00
Fe2+	0.58	0.53	0.49	0.47	0.47	0.47	0.47	0.47	0.47	0.47	0.49	0.59	0.48	0.48	0.55	0.57	0.60
Mn	0.01	0.01	0.01	0.01	0.01	0.01	0.01	0.01	0.01	0.01	0.01	0.01	0.01	0.01	0.01	0.01	0.01
Mg	1.36	1.41	1.46	1.48	1.50	1.49	1.48	1.50	1.49	1.50	1.45	1.37	1.47	1.47	1.38	1.39	1.34
Ca	0.03	0.03	0.02	0.02	0.02	0.02	0.03	0.01	0.02	0.01	0.02	0.04	0.01	0.03	0.03	0.03	0.03
Mg#	0.701	0.726	0.750	0.757	0.761	0.761	0.760	0.762	0.761	0.762	0.748	0.700	0.753	0.752	0.714	0.710	0.693

See Figure 6 for the location of points analyzed. Symbols used: o: interstitial orthopyroxene in the marginal zone, +: orthopyroxene in the core.

TABLE 2. COMPOSITIONAL VARIATION OF CUMULUS AND INTERSTITIAL ORTHOPYROXENE IN THE TWO SAMPLES FROM THE UG2 – MERENSKY REEF INTERVAL

Sample	1430.1 (norite)						1573.75 (anorthosite)						
						Std							Std
wt(%)	1	2	3	4	5		1	2	3	4	5	6	
SiO2	55.40	55.21	55.50	55.42	55.53	0.11	54.28	54.38	54.11	54.01	54.26	54.23	0.12
TiO2	0.23	0.22	0.22	0.26	0.23	0.02	0.14	0.23	0.28	0.26	0.27	0.14	0.06
Al2O3	1.01	1.07	1.03	1.05	1.00	0.03	0.53	0.82	0.81	0.79	0.86	1.20	0.20
Cr2O3	0.47	0.50	0.50	0.51	0.45	0.02	0.12	0.27	0.18	0.25	0.25	0.41	0.09
FeO	12.35	12.52	12.90	12.41	12.67	0.20	20.06	18.69	19.59	19.01	18.19	17.14	0.95
MnO	0.25	0.23	0.25	0.24	0.24	0.01	0.31	0.30	0.35	0.36	0.33	0.29	0.03
NiO	0.09	0.13	0.06	0.10	0.06	0.03	0.04	0.04	0.03	0.07	0.02	0.02	0.02
MgO	29.33	29.33	29.28	29.17	29.17	0.07	24.11	24.75	23.67	23.53	24.34	25.46	0.66
CaO	0.97	0.96	1.00	0.95	0.94	0.02	0.63	0.95	1.59	1.56	1.72	1.28	0.39
Na2O	0.00	0.00	0.00	0.01	0.01	0.00	0.01	0.00	0.03	0.02	0.01	0.03	0.01
Total	100.10	100.15	100.75	100.13	100.29	0.24	100.23	100.43	100.63	99.87	100.24	100.20	0.23
Cations (based on 6 atoms of oxygen)													
Si	1.97	1.96	1.96	1.97	1.97		1.99	1.98	1.98	1.99	1.98	1.97	
Ti	0.01	0.01	0.01	0.01	0.01		0.00	0.01	0.01	0.01	0.01	0.00	
Al	0.04	0.04	0.04	0.04	0.04		0.02	0.04	0.03	0.03	0.04	0.05	
Cr	0.01	0.01	0.01	0.01	0.01		0.00	0.01	0.01	0.01	0.01	0.01	
Fe	0.37	0.37	0.38	0.37	0.38		0.62	0.57	0.60	0.58	0.56	0.52	
Mn	0.01	0.01	0.01	0.01	0.01		0.01	0.01	0.01	0.01	0.01	0.01	
Mg	1.55	1.55	1.54	1.55	1.54		1.32	1.34	1.29	1.29	1.32	1.38	
Ca	0.04	0.04	0.04	0.04	0.04		0.02	0.04	0.06	0.06	0.07	0.05	
Mg#	0.809	0.807	0.802	0.807	0.804	0.001	0.682	0.702	0.683	0.688	0.705	0.726	0.015

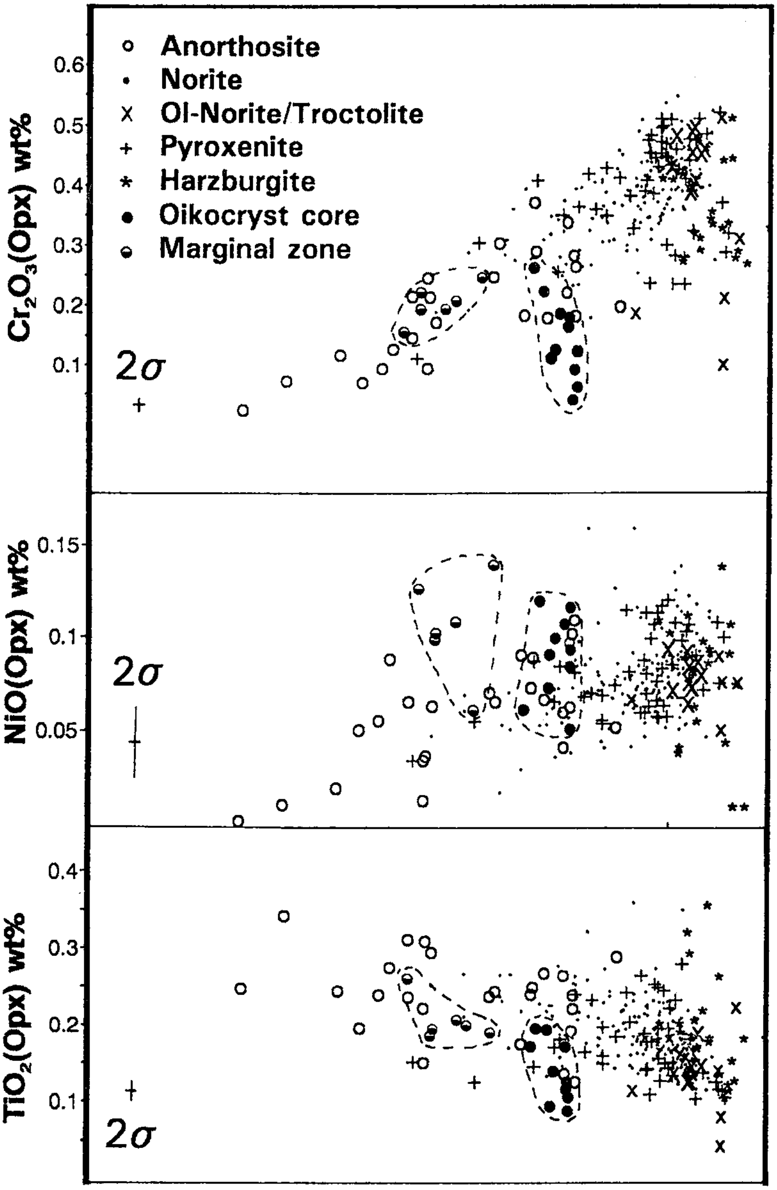

considerably more magnesian, although it does contain similar Ni concentrations (Fig. 4).

If compared with orthopyroxene from the Upper Critical Zone (Fig. 5), the orthopyroxene in the core of the mottle is markedly enriched in Al and depleted in Ti, Mn, and Cr. This is particularly apparent where orthopyroxene borders on olivine (Anal. 3 to 10, and 13, in Table 1, Fig. 6). Values of Mg# [= Mg/(Mg + Fe^{2+})] lie between 0.74 and 0.77 within the mottle. Orthopyroxene of the marginal zone plots within the compositional range of interstitial orthopyroxene in other examples of Bushveld anorthosite (Fig. 5). As a general pattern in cumulates from the Bushveld and other layered complexes, cumulus orthopyroxene shows much less variation within individual samples than interstitial orthopyroxene (Table 2).

Plagioclase in the olivine mottle is significantly more calcic (by *ca.* 15 mol.% An) than plagioclase in the host anorthosite, with plagioclase of the marginal zone having intermediate compositions (Table 3, Fig. 7). A relationship between grain size and composition is thus tentatively suggested. Generally,

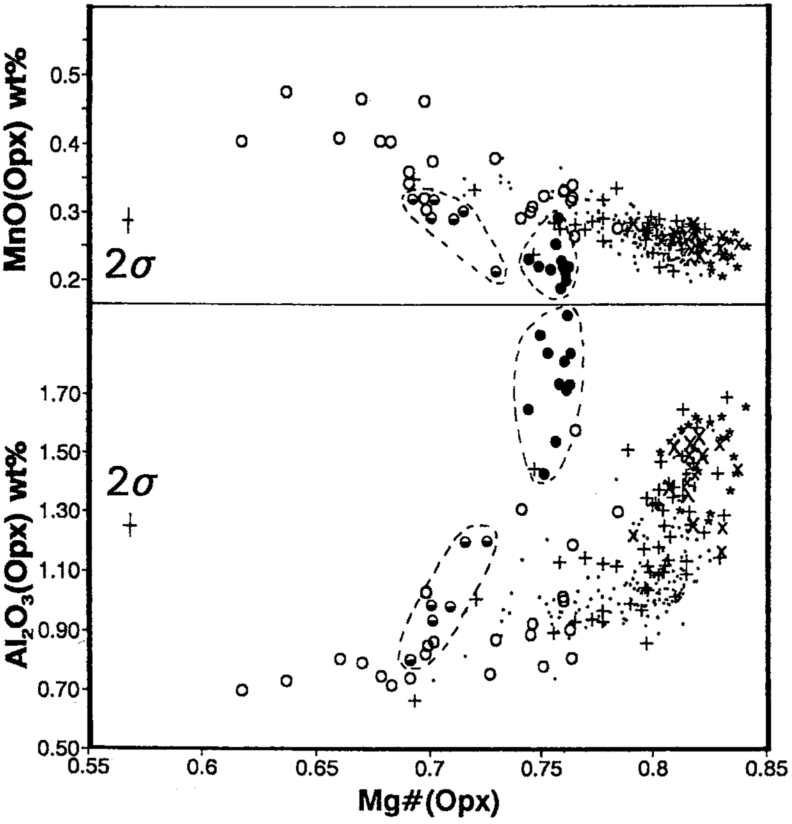

FIG. 5. Levels of Cr_2O_3, NiO, TiO_2, MnO and Al_2O_3 plotted against Mg# of orthopyroxene, based on electron-microprobe analysis of 250 samples from the UG2 – Merensky Reef interval (Maier 1992). Error bars denote 2σ standard deviation of analytical precision.

smaller cumulus grains show the highest An values in the Bushveld cumulates (Fig. 8). Fe and Sr contents of plagioclase, as determined by electron microprobe, are similar within and outside the olivine mottle (Fig. 7).

Both plagioclase inclusions in the oikocryst and cumulus plagioclase are typically reversely zoned (Fig. 8), but reversals tend to be more pronounced in the former. Reverse zoning is common in cumulus plagioclase of the Bushveld Complex; it may be observed in up to 80% of grains within norites and anorthosites of the UG2 – Merensky Reef interval (Maier 1994). Detailed analysis of cumulus plagioclase in the anorthosite under study indicates that (a) zonation seems to be superimposed on grain boundaries (Fig. 8), and (b) zonation is truncated and irregular (Fig. 9).

The amphibole in the marginal zone of the olivine mottle is hornblende with 46–51% SiO_2, 4.8–9.1% Al_2O_3, 10.3–12.4% FeO, 14.4–16.7% MgO, 12.3–12.7% CaO, and 0.45–0.98% Na_2O. The mica in the core of the olivine mottle is phlogopite, with 37.1–39.2% SiO_2, 15.3–17.0% Al_2O_3, 7.3–8.9% FeO,

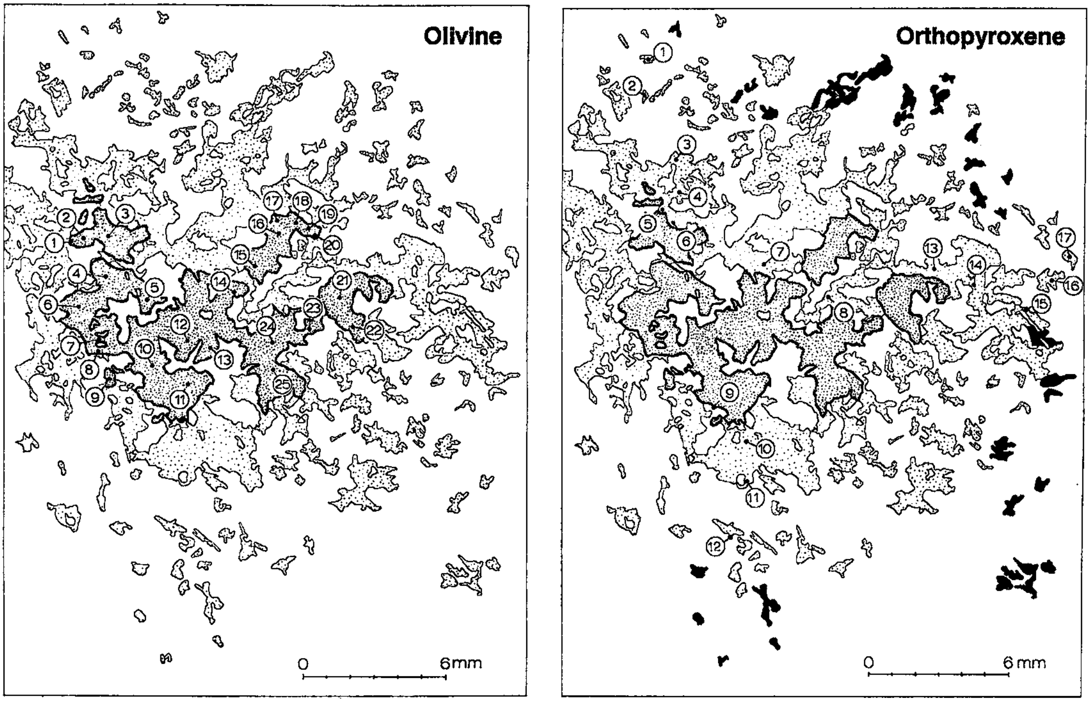

FIG. 6. Location of orthopyroxene and plagioclase analyzed in and around the olivine mottle. Olivine is shown in dense stipple, orthopyroxene in light stipple, plagioclase is colorless, and amphibole is solid. Numbers refer to Tables 1 and 3. Note that orthopyroxene described by analysis 9 is a narrow rim around olivine, and plagioclase described by analysis 18 is a small inclusion in olivine.

19.6–21.7% MgO, 0.32–0.46% Na_2O, and 5.15–5.66% K_2O. The unidentified fibrous phase found between plagioclase and olivine (Fig. 3b) has the following compositions: 24–29% SiO_2, 30.5–33.4% Al_2O_3, 12.8–15.2% FeO, 14.3–16.1% MgO, 6.2–6.7% CaO, 0.6–0.9% Na_2O.

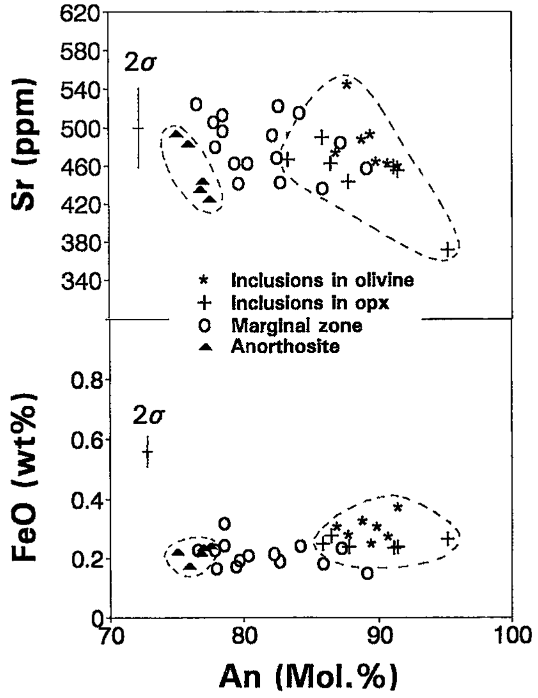

FIG. 7. Levels of Sr and FeO plotted against An content of plagioclase in the olivine mottle and the anorthosite. Errors depict 2σ standard deviation of analytical precision. Counting times for Sr were 200 s on peak and background. The counting error for Sr was determined by 54 analyses of an apatite standard containing 2300 ppm Sr.

TABLE 3. COMPOSITION OF PLAGIOCLASE IN AND AROUND THE OLIVINE MOTTLE

Analysis	1	2	3	4	5	6	7	8	9	10	11	12	13	14	15	16	17	18
Type	o	o	o	o	o	o	o	o	+	*	*	*	+	+	*	+	+	+
SiO2	49.25	49.46	48.77	46.96	47.72	47.92	47.76	47.57	45.61	45.41	45.95	46.53	45.28	47.25	46.17	47.08	46.37	44.02
Al2O3	31.96	31.68	32.10	33.57	33.00	32.93	32.97	33.26	34.30	33.98	34.08	33.60	34.51	32.83	33.93	33.37	33.87	35.15
FeO	0.23	0.16	0.24	0.19	0.23	0.22	0.25	0.25	0.24	0.36	0.30	0.27	0.25	0.97	0.32	0.26	0.25	0.27
CaO	15.65	15.39	15.87	17.32	16.84	16.47	16.92	17.08	18.40	18.25	18.22	17.80	18.37	16.76	18.09	17.47	17.77	19.30
Na2O	2.50	2.69	2.49	1.57	1.97	1.96	1.94	1.77	1.00	0.95	1.14	1.38	0.96	1.83	1.26	1.58	1.37	0.54
K2O	0.01	0.01	0.01	0.01	0.00	0.00	0.00	0.00	0.00	0.00	0.00	0.00	0.01	0.03	0.01	0.02	0.01	0.00
Total	99.59	99.39	99.47	99.61	99.76	99.50	99.84	99.93	99.54	98.95	99.68	99.57	99.37	99.68	99.78	99.78	99.64	99.28
Cations (based on 32 atoms of oxygen) :																		
Si	9.04	9.09	8.97	8.66	8.78	8.82	8.78	8.74	8.45	8.46	8.50	8.60	8.40	8.73	8.53	8.68	8.57	8.21
Al	6.91	6.86	6.96	7.30	7.16	7.15	7.15	7.20	7.49	7.46	7.43	7.32	7.55	7.15	7.39	7.25	7.38	7.73
Fe2+	0.03	0.02	0.04	0.03	0.04	0.03	0.04	0.04	0.04	0.06	0.05	0.04	0.04	0.15	0.05	0.04	0.04	0.04
Ca	3.08	3.03	3.13	3.42	3.32	3.25	3.33	3.36	3.65	3.65	3.61	3.53	3.65	3.32	3.58	3.45	3.52	3.86
Na	0.89	0.96	0.89	0.56	0.70	0.70	0.69	0.63	0.36	0.34	0.41	0.49	0.34	0.66	0.45	0.56	0.49	0.20
K	0.00	0.00	0.00	0.00	0.00	0.00	0.00	0.00	0.00	0.00	0.00	0.00	0.00	0.01	0.00	0.01	0.00	0.00
An	77.56	75.92	77.85	85.91	82.57	82.26	82.82	84.20	91.07	91.39	89.82	87.72	91.37	83.33	88.76	85.83	87.74	95.17
Sr (ppm)	420	478	508	439	472	495	446	518	461	457	461	541	457	468	484	492	446	374

Analysis	18	19	20	21	22	23	24	25	26	27	28	29	30	31	32	33	34	35
Type	+	o	*	o	+	o	*	*	o	o	o	o	o	o	o	o	o	o
SiO2	44.02	49.00	45.91	49.02	46.41	46.85	46.06	45.92	49.15	46.34	49.66	48.52	48.71	49.85	47.70	48.62	49.47	49.24
Al2O3	35.15	32.12	34.15	32.31	33.65	33.96	33.56	34.32	32.44	34.23	31.71	32.62	32.38	31.60	33.19	32.89	32.57	32.02
FeO	0.27	0.25	0.26	0.33	0.28	0.24	0.30	0.24	0.17	0.16	0.24	0.22	0.20	0.21	0.20	0.18	0.20	0.22
CaO	19.30	15.92	18.38	15.96	17.39	17.70	17.59	18.08	15.92	18.11	15.57	16.35	15.96	15.25	16.87	16.32	15.74	15.80
Na2O	0.54	2.40	1.04	2.40	1.50	1.42	1.46	1.18	2.47	1.22	2.63	2.20	2.25	2.80	1.93	2.29	2.58	2.54
K2O	0.00	0.01	0.01	0.02	0.01	0.01	0.02	0.01	0.02	0.00	0.01	0.01	0.00	0.01	0.03	0.06	0.08	0.10
Total	99.28	99.69	99.75	100.04	99.24	100.19	98.97	99.75	100.18	100.06	99.81	99.91	99.49	99.72	99.92	100.37	100.63	99.93
Cations (based on 32 atoms of oxygen) :																		
Si	8.21	8.99	8.49	8.97	8.60	8.60	8.57	8.48	8.97	8.53	9.09	8.90	8.95	9.13	8.76	8.88	8.99	9.02
Al	7.73	6.95	7.44	6.97	7.35	7.35	7.36	7.47	6.98	7.42	6.84	7.05	7.01	6.82	7.19	7.08	6.98	6.91
Fe2+	0.04	0.04	0.04	0.05	0.04	0.04	0.05	0.04	0.03	0.02	0.04	0.03	0.03	0.03	0.03	0.03	0.03	0.03
Ca	3.86	3.13	3.64	3.13	3.45	3.48	3.51	3.58	3.11	3.57	3.05	3.21	3.14	2.99	3.32	3.19	3.06	3.10
Na	0.20	0.85	0.37	0.85	0.54	0.51	0.53	0.42	0.88	0.43	0.93	0.78	0.80	0.99	0.69	0.81	0.91	0.90
K	0.00	0.00	0.00	0.00	0.00	0.00	0.00	0.00	0.00	0.00	0.00	0.00	0.00	0.00	0.01	0.01	0.02	0.02
An	95.17	78.56	90.65	78.56	86.47	87.25	86.88	89.41	77.98	89.13	76.57	80.38	79.71	75.04	82.67	79.45	76.81	77.01
Sr (ppm)	374	516	459	500	465	487	470	489	483	460	527	466	444	489	525	466	430	439

See Figure 6 for the location of points analyzed. Symbols used: o: plagioclase in anorthosite, +: inclusions in orthopyroxene, *: inclusions in olivine.

DISCUSSION

The problems encountered in the interpretation of cumulate textures were recently highlighted by McBirney & Hunter (1995). They summed up convincing evidence for *in situ* growth of cumulates followed by partial or complete recrystallization of the pile of crystals in the Skaergaard Intrusion (see also McBirney 1987, Boudreau 1987, Boudreau & McCallum 1992). Amongst other features, they observed poikilitic pyroxene, enclosing plagioclase grains of markedly reduced size, suggesting that growth of these grains was arrested upon entrapment by pyroxene, which crystallized simultanously with plagioclase at a crystallization front. In other words, in these authors' opinion, oikocrysts do not represent trapped liquid but are heteradcumulates. The general

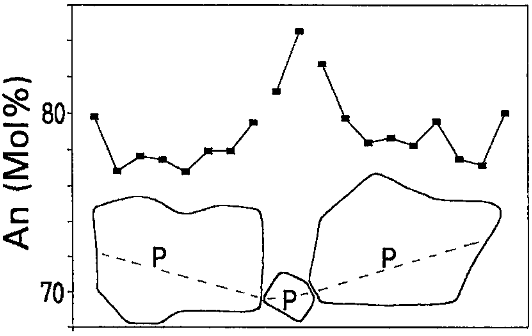

FIG. 8. Compositional zonation of three adjacent grains of plagioclase in anorthosite adcumulate.

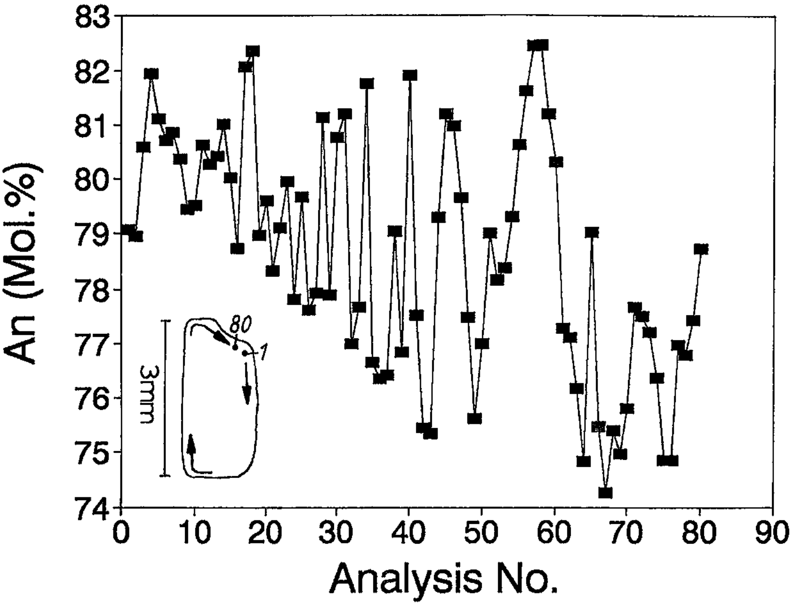

FIG. 9. Compositional variation in the rim zone of a plagioclase grain in anorthosite. Eighty analyses covering the circumference of the grain are spaced at a constant distance of 20 μm from the grain boundary.

paucity of late-stage phases such as quartz, amphibole and mica, as well as low concentrations of incompatible trace elements in anorthosites from the Stillwater Complex (Salpas *et al.* 1983), support this concept. The same paucity of late-stage phases and incompatible trace elements also is observed in anorthosites from the Bushveld Complex (Maier 1992).

In this study, I draw attention to a number of features that are inconsistent with a heteradcumulus origin of interstitial material in the Bushveld suite of anorthosite. (i) Compositions of interstitial orthopyroxene within any one sample of anorthosite are variable, especially in comparison with "cumulus" orthopyroxene found in norite or pyroxenite (Table 2). (ii) Comparison of the plagioclase inclusions in the olivine oikocrysts with "cumulus" plagioclase in the anorthosite (Fig. 7) shows substantial compositional and textural differences: the small rounded inclusions are strongly reversely zoned and enriched in the An component, whereas grains of plagioclase in the anorthosite are generally subhedral, much larger, depleted in An component and not as strongly zoned. (iii) Olivine of the mottle is richer in Fe than "cumulus" olivine of adjacent olivine norite, troctolite and harzburgite (Fig. 4). (iv) The olivine mottle contains abundant late-stage phases such as amphibole, mica, and minor quartz. Furthermore, concentrations of some trace elements that are incompatible with respect to the dominant phases, such as Zr, Rb, Zn, and Cu, are highly irregular in the Bushveld anorthosites (Maier 1992), an observation that has also been made for the Stillwater anorthosites by Salpas *et al.* (1983). These features suggest localized variation in melt composition, a condition typical of an interstitial environment, where convection and homogenization of the melt are less effective.

It is not possible to determine the composition of the interstitial "trapped" liquid, but a number of conditions can nevertheless be qualified. Morse & Nolan (1984) argued that strong reversals toward a Ca-rich rim on cumulus plagioclase in the Kiglapait Intrusion, Labrador, were caused by increased partition of Ca and Al into plagioclase owing to enrichment of the augite component in an intercumulus liquid. However, augite in general is a minor phase in the Lower and Critical Zones in the Bushveld Complex, and is entirely absent in the olivine mottle discussed here. Also, the shape of the inclusions suggests that resorption, rather than crystallization, was the dominant process prior to their entrapment by the ferromagnesian phases. Therefore, the mechanism of Morse & Nolan probably does not account for the reversals in plagioclase zoning and the high An contents described here.

Other chemical constituents that are enriched during fractional crystallization of a basaltic magma are incompatible trace elements such as K, Zr, Ti, and Rb, as well as H_2O. There is direct mineralogical evidence

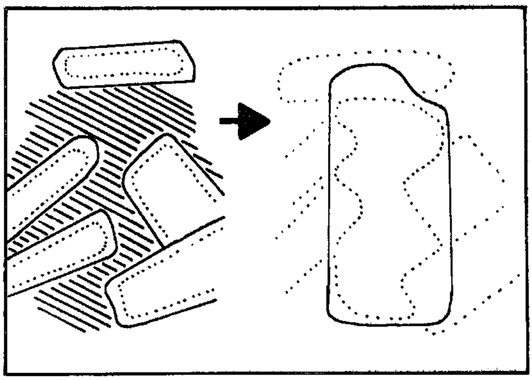

FIG. 10. Possible effects of grain-boundary migration on a plagioclase – melt assemblage, resulting in a grain like that in Fig. 9. Stippled contours indicate zoning.

for enrichment of both water and certain incompatible trace elements in the interstitial melt from which the olivine mottle crystallized, in the form of abundant mica and amphibole. Water is known to dramatically lower the liquidus temperatures of anhydrous phases, even in water-undersaturated systems (Robertson & Wyllie 1971, Whitney 1975). Accordingly, McBirney (1987) drew analogies between isothermal flux-melting as a result of water enrichment in metallurgical refining of ingots and in a semiconsolidated pile of cumulates.

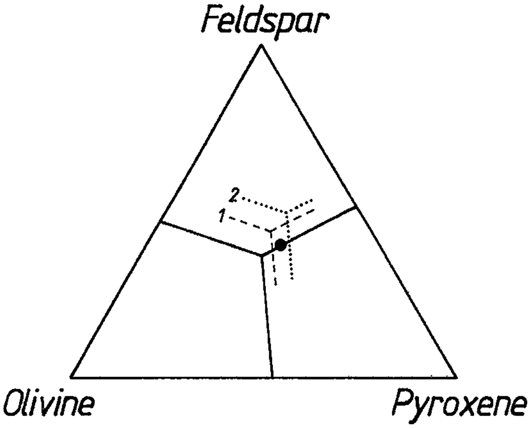

FIG. 11. Schematic diagram, showing shift in liquidus position within the system feldspar – olivine – pyroxene in response to addition of water [modified after Kushiro (1975) and McBirney (1987)]. Solid dot represents possible composition of interstitial melt generally of noritic character.

In the case of plagioclase, water enrichment may cause preferential dissolution of the albite component in the melt, leading to a Ca-enriched rim (Boudreau 1988). Panjasawatwang *et al.* (1995) documented that an increase in the H_2O content of both H_2O-undersaturated and saturated melts enhances Ca partition into plagioclase. Considering additional evidence, such as the truncation of compositional zoning in plagioclase (Fig. 9), and the fact that up to 80% of the grains of cumulus plagioclase within the UG2 – Merensky Reef interval of the Bushveld Complex are reversely zoned (Maier 1994), I believe that resorption was a widespread phenomenon in the interstitial regime. The occurrence of the highest An contents in the smallest grains of plagioclase and the continuity of compositional trends across grain boundaries (Fig. 8) also suggest that the zonation is a postcumulus phenomenon. However, it should be noted that, following Means & Park (1994), zoning patterns in general may have to be reinterpreted. Accordingly, the truncation shown in Figure 9 and that in the study by Singer & Pearce (1993) may have formed by grain-boundary migration, as schematically shown in Figure 10.

Another phase in the mottle of rather unusual composition is orthopyroxene. It is enriched in Al, and depleted in Cr, Ti, and Mn near olivine. The Al enrichment, in particular, cannot have been caused by subsolidus reaction between the two phases, or reaction replacement of olivine by orthopyroxene, as Al contents of olivine are negligible. Therefore, I propose that orthopyroxene reacted with (and, on the basis of textural evidence, was possibly resorbed by) a melt enriched in Al and depleted in Cr, Ti, and Mn. A late-stage melt enriched in the albite and anorthite component owing to partial resorption of plagioclase would be a possible parent. Resorption of orthopyroxene and crystallization of olivine may be explained by a shift in stability fields of the phases (Fig. 11). This could have been triggered by enrichment of the interstitial melt in (i) water (Kushiro 1972), in response to fractionation and compaction of the pile of cumulates, or (ii) Na, in response to resorption of plagioclase (Kushiro 1975). Establishment of the relative timing of crystallization and resorption of the individual phases is not attempted here, particularly since Means & Park (1994) have shown that supersolidus phase-boundary migration may be an important phenomenon in plutonic systems.

CONCLUSIONS

In this study, I have presented evidence that olivine mottles are a product of crystallization of a relatively hydrous interstitial melt. It is clear that olivine mottles are relatively rare, compared to pyroxene mottles. The two types of mottles may reflect different degrees of compositional exchange between the semiconsolidated pile of cumulates and the main body of magma. Hence, whereas orthopyroxene mottles could represent a relatively water-poor regime, migration of interstitial melt was apparently limited in certain cases, resulting in localized enrichment of water and incompatible trace elements and the crystallization of olivine and hydrous phases. Significantly, plagioclase inclusions in pyroxene mottles are generally larger, but less rounded, embayed, calcic and reversely zoned than inclusions in the olivine mottle studied here (Fig. 3f).

The mechanism by which melt migration in the pile of cumulates was upheld remains enigmatic. It has been argued that resorption was a widespread phenomenon in the interstitial regime. It is possible that resorption, in keeping channelways open for melt migration, facilitated compaction of cumulates and expulsion of interstitial melt. However, more detailed investigations, involving Nomarski microscopy (*cf.* Singer & Pearce 1993), in combination with electron-microprobe analyses, are needed before the viability of this process can be estimated with a greater degree of confidence.

ACKNOWLEDGEMENTS

The Foundation for Research Development of South Africa, the Rhodes University Joint Committee for Research, and NSERC (Canada) are thanked for financial support. Messrs. Genmin provided the sample material and gave logistical support. Julian Marsh and two referees are thanked for improving an early draft of the manuscript.

REFERENCES

BOUDREAU, A.E. (1987): Pattern formation during crystallization and the formation of fine-scale layering. *In* Origins of Igneous Layering (I. Parsons, ed.). D. Reidel, Dordrecht, The Netherlands (453-472).

________ (1988): Investigations of the Stillwater Complex. IV. The role of volatiles in the petrogenesis of the J–M Reef, Minneapolis Adit section. *Can. Mineral.* **26**, 193-208.

________ & MCCALLUM, I.S. (1992): Infiltration metasomatism in layered intrusions – an example from the Stillwater Complex, Montana. *J. Volc. Geotherm. Res.* **52**, 171-183.

KUSHIRO, I. (1972): Effect of water on the compositions of magmas formed at high pressures. *J. Petrol.* **13**, 311-334.

________ (1975): On the nature of silicate melt and its significance in magma genesis: regularities in the shift of the liquidus boundaries involving olivine, pyroxene, and silica minerals. *Am. J. Sci.* **275**, 411-431.

MAIER, W.D. (1992): *Geochemical and Petrological Trends in the UG2 – Merensky Unit Interval of the Upper Critical Zone in the Western Bushveld Complex.* Ph.D. thesis, Rhodes Univ., Grahamstown, South Africa.

________ (1994): Grain-size variations of cumulus plagioclase in the Upper Critical Zone of the Bushveld Complex. *Mineral. Petrol.* **50**, 245-258.

MATHISON, C.I. (1987): Pyroxene oikocrysts in troctolitic cumulates – evidence for supercooled crystallization and postcumulus modification. *Contrib. Mineral. Petrol.* **97**, 228-236.

MCBIRNEY, A.R. (1987): Constitutional zone refining of layered intrusions. In *Origins of Igneous Layering* (I. Parsons, ed.). D. Reidel, Dordrecht, The Netherlands (437-452).

________ & HUNTER, R.H. (1995): The cumulate paradigm reconsidered. *J. Geol.* **103**, 114-122.

________ & NOYES, R.M. (1979): Crystallization and layering of the Skaergaard Intrusion. *J. Petrol.* **20**, 487-554.

MEANS, W.D. & PARK, Y. (1994): New experimental approach to understanding igneous texture. *Geology* **22**, 323-326.

MORSE, S.A. & NOLAN, K.M. (1984): Origin of strongly reversed rims on plagioclase in cumulates. *Earth Planet. Sci. Lett.* **68**, 485-498.

PANJASAWATWONG, Y., DANYUSHEVSKY, L.V., CRAWFORD, A.J. & HARRIS, K.L. (1995): An experimental study of the effects of melt composition on plagioclase – melt equilibria at 5 and 10 kbar: implications for the origin of magmatic high-An plagioclase. *Contrib. Mineral. Petrol.* **118**, 420-432.

RAEDEKE, L.D. & MCCALLUM, I.S. (1980): A comparison of fractionation trends in the lunar crust and the Stillwater Complex. *In* Proc. Conf. Lunar Highlands Crust (R.B. Merrill & J.J. Papike, eds.). *Geochim. Cosmochim. Acta, Suppl.* **12**, 133-153.

ROBERTSON, J.K. & WYLLIE, P.J. (1971): Rock–water systems, with special reference to the water-deficient region. *Am. J. Sci.* **271**, 252-277.

SALPAS, P.A., HASKIN, L.A. & MCCALLUM, I.S. (1983): Stillwater anorthosites: a lunar analog? *In* Proc. 14th Lunar Planet. Sci. Conf. *J. Geophys. Res., Suppl.* **88**, B27-B39.

SINGER, B.S. & PEARCE, T.H. (1993): Plagioclase zonation in a basalt to rhyodacite eruptive suit, Seguam Island, Alaska: observations by Nomarski contrast interference. *Can. Mineral.* **31**, 459-466.

WAGER, L.R. & BROWN, G.M. (1968): *Layered Igneous Rocks.* Oliver and Boyd, Edinburgh, U.K.

________, ________ & WADSWORTH, W.J. (1960): Types of igneous cumulates. *J. Petrol.* **1**, 73-85.

WHITNEY, J.A. (1975): The effects of pressure, temperature and X_{H2O} on phase assemblage in four synthetic rock compositions. *J. Geol.* **83**, 1-31.

Received March 24, 1995, revised manuscript accepted June 20, 1995.